Tennessee 37921.
[1]I. R. Williams and C. B. Fulmer, Phys. Rev. 154, 1005 (1967).
[2]I. R. Williams and C. B. Fulmer, Phys. Rev. 162, 1055 (1967).
[3]D. W. Sheffey, I. R. Williams, and C. B. Fulmer, Phys. Rev. 172, 1094 (1968).
[4]J. W. Clark, C. B. Fulmer, and I. R. Williams, Phys. Rev. 179, 1104 (1969).
[5]C. B. Fulmer and I. R. Williams, Nucl. Phys. A155, 40 (1970).
[6]J. P. Hazan and M. Blann, Phys. Rev. 137, B1202 (1965).
[7]C. M. Lederer, J. M. Hollander, and I. Perlman, *Table of Isotopes* (Wiley, New York, 1967), 6th ed.
[8]E. A. Bryant, D. F. R. Cochran, and J. D. Knight, Phys. Rev. 130, 1512 (1963).
[9]K. H. Purser and E. W. Titterton, Australian J. Phys. 12, 103 (1959).
[10]S. Kaufman, Phys. Rev. 117, 1532 (1960).
[11]B. L. Cohen, E. Newman, T. H. Handley, Phys. Rev. 99, 723 (1955).
[12]F. S. Houck and J. M. Miller, Phys. Rev. 123, 231 (1961).
[13]J. H. Carver and W. Turchinetz, Proc. Phys. Soc. (London) 73, 585 (1959).
[14]E. L. Callis, Oak Ridge National Laboratory Report No. ORNL-TM-2309, 1968 (unpublished).
[15]M. Blann and A. Ewart, Phys. Rev. 134, B783 (1964).
[16]L. C. Northcliffe and R. F. Schilling, Nucl. Data A7, 233 (1970).
[17]K. Eskola, Physics Letters 23, 471 (1966).
[18]J. M. Black, W. C. McHarris, and W. H. Kelley, Phys. Rev. Letters 26, 451 (1971).
[19]I. Dostrovsky, Z. Fraenkel, and G. Friedlander, Phys. Rev. 116, 683 (1959).
[20]P. C. Rogers, Ph.D. thesis, Massachusetts Institute of Technology, 1962 (unpublished).
[21]V. F. Weisskopf, Phys. Rev. 52, 295 (1937).
[22]J. R. Huizenga and R. Vandenbosch, Phys. Rev. 120, 1305, 1313 (1960).
[23]W. L. Hafner, J. R. Huizenga, and R. Vandenbosch, Argonne National Laboratory Report No. ANL-6662, 1962 (unpublished).
[24]I. R. Williams and K. S. Toth, Phys. Rev. 138, B382 (1965).
[25]J. R. Beyster, Los Alamos Scientific Laboratory Report No. LA-2094, 1957 (unpublished).
[26]F. G. Perey, unpublished.
[27]I. Halpern, R. J. Debs, J. T. Eisinger, A. W. Fairhall, and H. G. Richter, Phys. Rev. 97, 1327 (1955).
[28]C. B. Fulmer, K. S. Toth, I. R. Williams, T. H. Handley, G. F. Dell, E. L. Callis, and T. M. Jenkins, Phys. Rev. C 2, 1397 (1970).

PHYSICAL REVIEW C VOLUME 6, NUMBER 5 NOVEMBER 1972

# Neutron Decay from the $^{49}$Ca Ground-State Analog in $^{49}$Sc†

A. J. Elwyn, F. T. Kuchnir,* J. E. Monahan,‡ F. P. Mooring, and J. F. Lemming§
*Argonne National Laboratory, Argonne, Illinois 60439*

and

W. G. Stoppenhagen
*Ohio University, Lancaster, Ohio 43130*
(Received 5 July 1972)

Relative angular distributions of neutrons from the $^{48}$Ca$(p,n)$ $^{48}$Sc reaction to four positive-parity states in $^{48}$Sc have been measured at 11 proton energies between 1.955 and 1.995 MeV. This energy interval encompasses a number of the components of the $\frac{3}{2}^-$ isobaric analog of the $^{49}$Ca ground state in $^{49}$Sc. The neutron decay of $^{49}$Sc in the region of the two largest components is discussed in terms of a model of the $(p,n)$ reaction in which the isospin-violating forces are assumed to manifest themselves through boundary-condition mixing only. The gross features of most of the data throughout this energy interval can be described in terms of two $T_<$ $\frac{3}{2}^-$ states and a number of $\frac{3}{2}^+$ and $\frac{5}{2}^+$ levels. The branching ratio for neutron decay to the various levels in $^{48}$Sc suggests that the two major $\frac{3}{2}^-$ components have fairly simple but somewhat different shell-model configurations.

## I. INTRODUCTION

Analog-resonant $(p, n)$ reactions to low-lying states in the residual nucleus are usually isospin forbidden. The resonance reaction occurs only through the mixing of the analog with a "background" of compound-nucleus states of the same spin and parity as that of the analog state but with isospin $T_<$ one unit less than the isospin $T_>$ of the analog. For many nuclei the density of $T_<$ levels at analog-state excitation energies is sufficiently large that the background levels can be treated statistically.[1] For the $^{48}$Ca$(p, n)^{48}$Sc reaction, however, at proton energies corresponding to an

excitation of ~11.6 MeV in $^{49}$Sc, the $^{49}$Ca $\frac{3}{2}^-$ ground-state analog is split[2-5] into a number of non-overlapping fine-structure components each with $J^\pi = \frac{3}{2}^-$.[6] The present investigation is concerned with properties of the neutron decay from some of these components to four final states in $^{48}$Sc.

An $R$-matrix description of $(p, n)$ reactions through analog resonances in the case of non-overlapping $T_<$ states has been given by Mello[7] and, in a more general form, by Robson and Lane.[8] Two equivalent expressions for the $(p, n)$ collision-matrix elements are obtained. In one expression the effects of the analog on the $T_<$ states are calculated explicitly, whereas in the second the effects of the $T_<$ states on the analog are explicit.

In the present report we specialize the first form to the case of a single analog state with a background of a few non-overlapping $T_<$ states in order to analyze the neutron angular distributions observed in the $^{48}$Ca$(p, n)^{48}$Sc reaction. The measured distributions are compared with calculations based on this model, and neutron branching ratios for decay from the two major fine-structure components in $^{49}$Sc to the $5^+$, $4^+$, $3^+$, and $2^+$ final states[9] in $^{48}$Sc are determined.

The low-lying positive-parity states of $^{48}$Sc can be described[9] as relatively pure $(\pi 1f_{7/2}, \nu 1f_{7/2}^{-1})$ shell-model configurations. Enhancement of neutron decay to such states occurs through those $T_<$ compound-nucleus levels that mix strongly with the analog state, which is known to be predominately a 2p-1h state $(\pi 1f_{7/2}, \nu 1f_{7/2}^{-1} 2p_{3/2})$. Wilhjelm *et al.*[6] have suggested that the two largest $\frac{3}{2}^-$ fine-structure components associated with the analog are of relatively simple 3p-2h character. A similar conclusion has been tentatively suggested by Chasman *et al.*[5] in a study of the $^{48}$Ca$(p, \gamma)^{49}$Sc reaction. In the present study the neutron branching ratios for the decay of these two $\frac{3}{2}^-$ components to several final states in $^{48}$Sc are obtained from the analysis of the differential cross sections, and are discussed in terms of the possible structure of these $T_<$ components.

In the experiment, the relative differential cross sections of the neutrons associated with four final $^{48}$Sc states are measured[10] by time-of-flight techniques employing the pulsed and bunched proton beam from the Dynamitron accelerator. Although the $^{49}$Ca ground state analog has been studied extensively in a variety of proton-induced reactions,[2-6,11] there have been few investigations[4,12] of the neutron decay to individual final states, and no previous detailed angular distribution experiments.

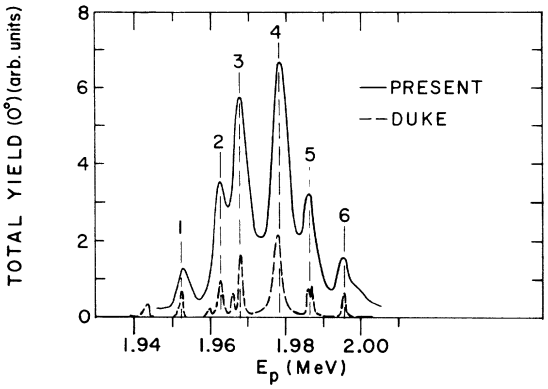


FIG. 1. Total 0° neutron yield in the $^{48}$Ca$(p,n)^{48}$Sc reaction, plotted as a function of incident proton energy. The solid curve represents data obtained with an over-all energy resolution of about 4 keV. The dashed curves are the results of Ref. 6, except that the energy scale has been shifted 4 keV toward higher energies to match the calibration of the present results.

## II. EXPERIMENTAL PROCEDURE

The experiment was carried out at the Argonne 4-MV Dynamitron accelerator equipped with a pulsed and bunched ion source. Proton beam

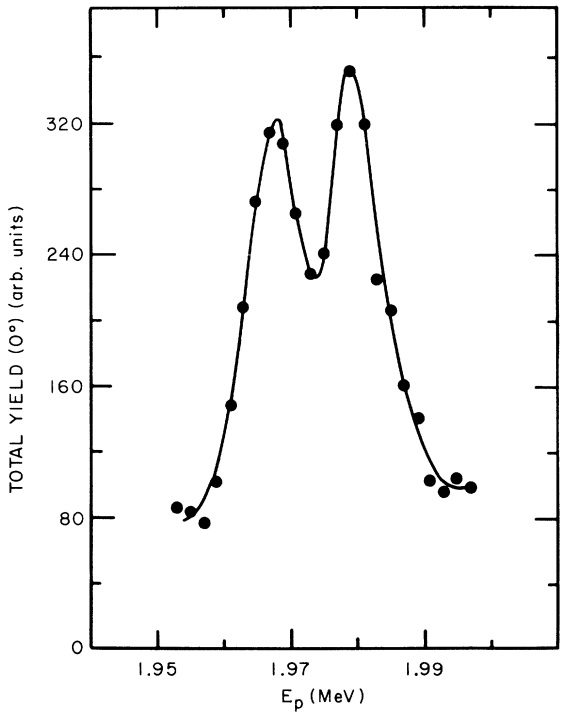


FIG. 2. Total neutron yield in the $^{48}$Ca$(p,n)^{48}$Sc reaction, as measured at 0°. The data, which are plotted as a function of incident proton energy, were obtained with an over-all energy resolution width of about 8 keV. The solid curve is drawn to guide the eye.

bursts of 1.5–1.8 nsec full width at half maximum (FWHM) with peak currents of 2–3 mA, at a 1-MHz repetition rate were utilized in these measurements. The accelerator voltage, and hence the energy of the proton beam, was measured and controlled by directing the $H_2^+$ beam into a 90° electrostatic analyzer which was calibrated with respect to the $^7$Li$(p, n)^7$Be threshold. The $^{48}$Ca targets were prepared by vacuum evaporation of $CaCO_3$ (enriched to 95.6% in $^{48}$Ca) onto thick tantalum backings. The target was supported on an O-ring seal at the end of an aluminum can which also acted as a Faraday cup. A conventional low-input-impedance current integrator and a standard long counter were used as monitors. A jet of compressed air cooled the target, which was rotated at about 1 rev/sec about the incident proton beam so that the beam spot described a circle 2 in. in diameter.

Measurements were taken at proton beam energies from 1.955 to 1.995 MeV in steps of 4 keV. The total $(p, n)$ yield in this energy region was obtained at 0° by use of a long counter; the over-all energy resolution width was about 4 keV. The results (Fig. 1) show six peaks at approximately 1.953, 1.963, 1.968, 1.978, 1.986, and 1.995 MeV. The dashed curve, shown for comparison, represents data[13] taken with much better energy resolution and shows additional structure. Eight of the almost-resolved peaks have been identified[6] as $\frac{3}{2}^-$ resonances and are interpreted as the fine-structure components associated with the splitting of the $\frac{3}{2}^-$ $^{49}$Ca ground-state analog.

In the angular-distribution measurements, a thicker $^{48}$Ca target (~8 keV thick) was used. The total 0° neutron yield from this target is shown in Fig. 2. Two large peaks, at about 1.965 and 1.975 MeV, are observed. This doublet is similar to that observed by Jones *et al.*[2] and apparently should be associated primarily with the two largest components labeled 3 and 4 in Fig. 1.

Differential cross sections for $^{48}$Ca$(p, n)^{48}$Sc reactions to the various final states in $^{48}$Sc were determined by time-of-flight measurements of the neutron groups corresponding to these states. The use of four detectors, each of which was a cylindrical stilbene scintillator 1 in. long and 2 in. in diameter directly coupled to an RCA-8575 photomultiplier, allowed simultaneous measurements at four angles. Each counter assembly was supported by a wedge-shaped arm which could rotate about a pivot directly below the target position, and it could also slide along the arm to adjust the flight path from 0.5 to 2.0 m. The final data were taken with the detector placed 1 m from the target. This was found to be sufficient to resolve the neutron groups.

The main features of the electronic instrumentation are shown schematically in Fig. 3, which for simplicity shows only the input from neutron de-

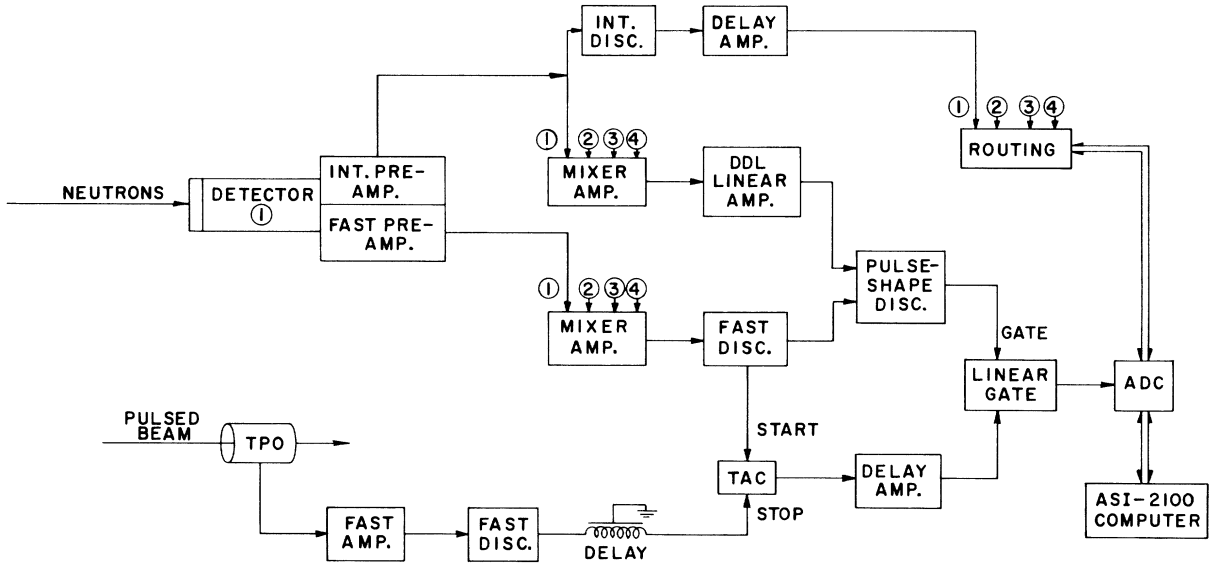


FIG. 3. Block diagram of the time-of-flight electronics. For simplicity, only neutron detector No. 1 and its input circuit are shown. The points at which the input circuits of the other three detectors feed into the main circuit are indicated by the circled numbers 2, 3, and 4. In this figure TPO is the time-pickoff in the proton beam line, TAC the time-to-amplitude converter, DDL Linear Amp. is a double-delay line amplifier, INT stands for integral, and ADC is the analog-to-digital converter.

tector No. 1 and merely uses the circled numbers 2, 3, and 4 to show the points at which the input circuits of the other three detectors feed in. A time-to-amplitude converter (TAC) is used to measure the time interval between signals from the neutron detectors and from a capacitive time pickoff (TPO) placed in the proton beam about 1 m from the target. The $\gamma$-ray background was reduced by use of pulse-shape discrimination circuitry[14] in which the time interval between the signal from the fast-start discriminator and the crossover point of a clipped signal from the double-delay-line (DDL) linear amplifier is measured. When this discriminator has identified a detected particle as a neutron, it opens a linear gate which allows the time-of-flight information to pass to the analog-to-digital converter (ADC). At the same time, a signal coming from the neutron detector causes the routing circuit to add two bits to the address of the ADC information in order to indicate the neutron detector from which the signal came. Thus the time spectrum associated with each of the four neutron detectors is stored in a separate section of the 4000-channel memory. An ASI-2100 computer with an 8000-word memory is used on line for preliminary data reduction.

The time calibration, linearity, and counting-rate stability of the TAC were checked by use of a precision time calibrator.[15] The intrinsic time resolution of the electronic equipment, as measured with annihilation $\gamma$ coincidences from a $^{68}$Ge source, was about 0.8 nsec. One of the limiting factors in over-all time resolution is the spread of the beam pulses from the bunching system. The observed resolution width in the $\gamma$-ray peak is 1.8–2 nsec FWHM. This implies that the pulsed-beam contribution was of the order of 1.5–1.8 nsec.

A typical time-of-flight spectrum is shown in Fig. 4. The time dispersion is 0.46 nsec/channel. The spectrum was measured at 0° at a bombarding energy of 1.975 MeV. Neutron groups $n_1$, $n_2$, $n_3$, and $n_4$ correspond to transitions leading to the first four excited states in $^{48}$Sc at 0.131, 0.252, 0.624, and 1.144 MeV, respectively. An asymmetry in line shape can be seen (Fig. 4) in the form of a low-energy tail. This effect is caused mainly by some time walk at low pulse heights (a dynamic range of 20 : 1 was accepted). Air scattering and target thickness can also contribute to the tail. Because of the nonlinear variation of neutron energy with flight time, the resolution improves rapidly with decreasing neutron energy. The over-all energy resolution (FWHM) is 70 keV for the high-energy doublet ($n_1$ and $n_2$, with $E_n \approx 1.25$ MeV) and 20 keV for the lowest-energy group ($n_4$, with $E_n \approx 270$ keV). All integral discriminators were set below the lower-level discriminator of the timing single-channel analyzer (TSCA) in the pulse-shape discrimination circuit which is common to all four channels. This discriminator, therefore, determined the detection efficiency, and it was set so that the threshold for detection corresponded to a neutron energy of about 100 keV. For optimum performance, the upper-level discriminator of the TSCA was set at a level corresponding to the Compton edge of the 0.360-keV line of $^{233}$Ba. From previous calibration[14] this is known to correspond to the maximum pulse height for protons recoiling after the scattering of ~1.4-MeV neutrons.

The relative efficiency of each of the four neutron detectors was determined by comparing its response to neutrons of a given energy from the $^7$Li$(p, n)^7$Be reaction with that of a standard long counter. The gains and other settings of the electronics were adjusted so the differences among their efficiencies were at most ~10%. Since the flat response of the long counter had been confirmed by use of several standard neutron sources, the energy dependence of the efficiency of each detector was readily determined by use of the known[16] cross section of the $^7$Li$(p, n)^7$Be reaction. These calibrations enabled us to correct the data for all variations in the relative efficiencies of the detectors. Because the thickness of the lithium target

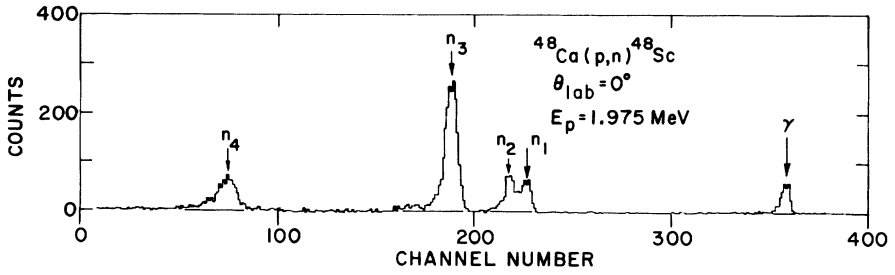


FIG. 4. Neutron time-of-flight spectrum obtained at an incident proton energy of 1.975 MeV at an angle of 0°. The flight path was 1 m and the time dispersion was 0.46 nsec/channel. The arrows mark the $\gamma$-ray peak ($\gamma$) and the various neutron groups ($n_1$–$n_4$), as discussed in the text. Spectra obtained at other energies and angles are similar.

was not known, absolute detector efficiencies could not be obtained.

The background at the detectors was evaluated by intercepting the direct neutron beam with a Lucite absorber placed between the target and each detector and also by using a blank tantalum target in place of the Ca sample. It was found that the background associated with the $^{48}$Ca target itself was flat and negligible. Some time-correlated neutron background, later associated with the beam hitting a Cu beam-line reducer, was observed at backward angles only. Because of its characteristic time correlation, this background was easily subtracted out.

Most of the angular-distribution data were collected over a 3-day period with the same $^{48}$Ca target. The total neutron yield from the target was checked each day over the entire proton energy range of interest. Over the 3-day period, the peak positions shifted about 1.5 keV. This shift was attributed to carbon deposition on the target, and was considered to be negligible relative to the target thickness.

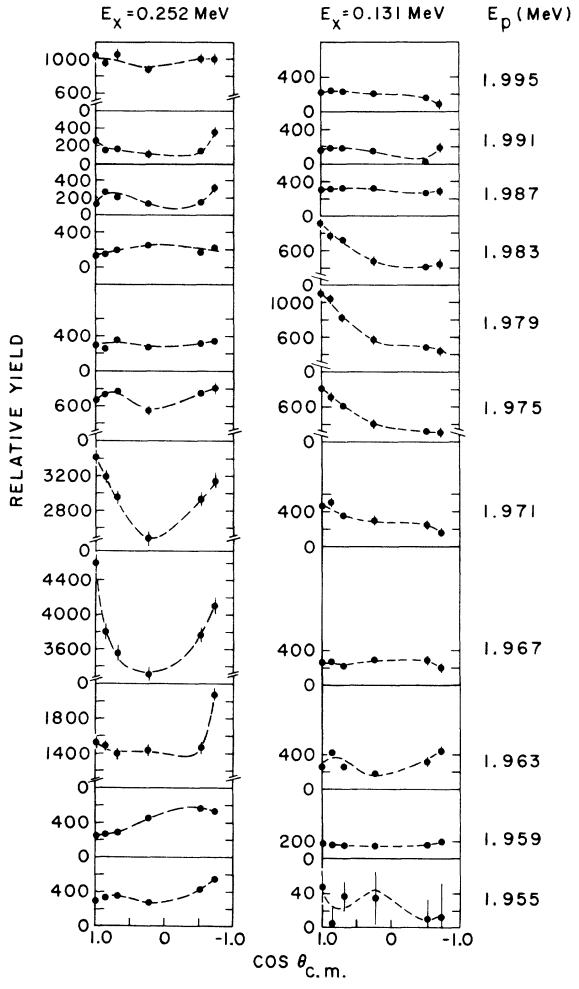


FIG. 5. Relative differential cross sections in the c.m. system as a function of $\cos\theta_{c.m.}$ for the neutron groups corresponding to the excitation of the $5^+$ (0.131-MeV) state and the $4^+$ (0.252-MeV) state in $^{48}$Sc in the $^{48}$Ca$(p,n)$ reaction at the indicated incident energies $E_p$. The smooth curves are drawn only to guide the eye.

Angular distributions were measured for eleven proton energies at six angles between 0 and 135°. In each time-of-flight spectrum, four neutron groups – $n_1$, $n_2$, $n_3$, and $n_4$ in Fig. 4 – were identified and were assigned, as mentioned previously, to transitions leading to the first four excited states in $^{48}$Sc at excitation energies 0.131, 0.252, 0.624, and 1.144 MeV, respectively. In none of the data is there evidence for a neutron transition to the ground state ($J^\pi = 6^+$), to the known[9] $J^\pi = 7^+$ state at 1.096 MeV, nor to the negative-parity (probably $2^-$) state[9,17] at 1.402 MeV.

The intensity of isolated peaks ($n_3$ and $n_4$) was found by summing the contents of the relevant channels and subtracting the background. To obtain the net yield to each of the two unresolved neutron groups ($n_1$ and $n_2$), an unfolding procedure was used.[18] For such an analysis, a standard line shape is needed. Since the line shapes of time-of-flight spectra are complicated functions of experimental parameters, a simple analytical peak shape is inappropriate. Our approach has been to use the strong isolated neutron group $n_3$ as a reference standard. The three groups ($n_1$, $n_2$, and $n_3$) were fitted simultaneously and the goodness of fit for the isolated group was used as a measure of the correctness of the standard line shape.

## III. RESULTS

Although the measured yield at each angle and energy was corrected for the relative detector efficiency, no absolute cross sections were obtained. In Figs. 5 and 6, the relative differential cross sections of the four neutron groups are shown at each of the 11 proton energies $E_p$. The coefficients $B_0, \ldots, B_4$ in an expansion of the differential cross section into a series of Legendre polynomials are displayed in Figs. 7 and 8.

For the 0.252-MeV ($4^+$), 0.624-MeV ($3^+$), and the 1.144-MeV ($2^+$) final states, the total yield (as represented by the coefficient $B_0$) is dominated by a peak near a proton energy of 1.965 MeV – the energy region associated with the lower energy peak of the doublet observed in Fig. 2; resonances in the region of the higher-energy component apparently contribute very little to the yield to these positive-parity final states. In the reaction proceeding to the $5^+$ state at 0.131 MeV, the relative yields throughout are quite small; at energies

near 1.965 MeV the intensity is about $\frac{1}{30}$ of that to the $2^+$ state.

The angular distributions, particularly in the decay to the 0.131- and 0.624-MeV final states, are in general asymmetric about 90°, as indicated by the nonzero values of the odd-order Legendre-polynomial coefficients. The existence of such odd-order coefficients implies that there is interference between odd and even partial waves participating in the reaction. Since $T_<$ compound-nucleus states associated with the $^{49}$Ca ground-state isobaric analog resonance have $J^\pi = \frac{3}{2}^-$, nonzero values for the coefficients $B_1$ and $B_3$ indicate that positive-parity levels in the compound nucleus $^{49}$Sc are being excited as well.

Both the $2^+$ (1.144-MeV) and $3^+$ (0.624-MeV) final states are reached predominantly via $p$-wave neutron emission from the $\frac{3}{2}^-$ compound-nucleus levels. Since the odd-order coefficients associated with the $2^+$ state are small, the reaction is probably dominated by resonant decay from such $\frac{3}{2}^-$ states. For neutron decay to the $3^+$ state, on the other hand, large values of $B_1$ indicate that positive-parity levels participate strongly (at least at certain energies). In the case of neutron decay from $\frac{3}{2}^-$ levels to the $4^+$ (0.252-MeV) and $5^+$ (0.131-MeV) states, the reaction proceeds via $f$-wave neutrons. On the basis of calculated neutron and proton penetrabilities alone, the yield to the $5^+$ state in such decay should be only about $\frac{1}{30}$ of that to the $2^+$ state at $E_p = 1.965$ MeV, in good agreement with the observations mentioned above. Thus, at energies near 1.965 MeV the reaction to the $5^+$ state is in all likelihood dominated by $\frac{3}{2}^-$ resonant states. At higher proton energies the relatively large values of the coefficient $B_1$ indicate the participation of positive-parity resonances. For the $4^+$ state, on the other hand, calculated values of neutron

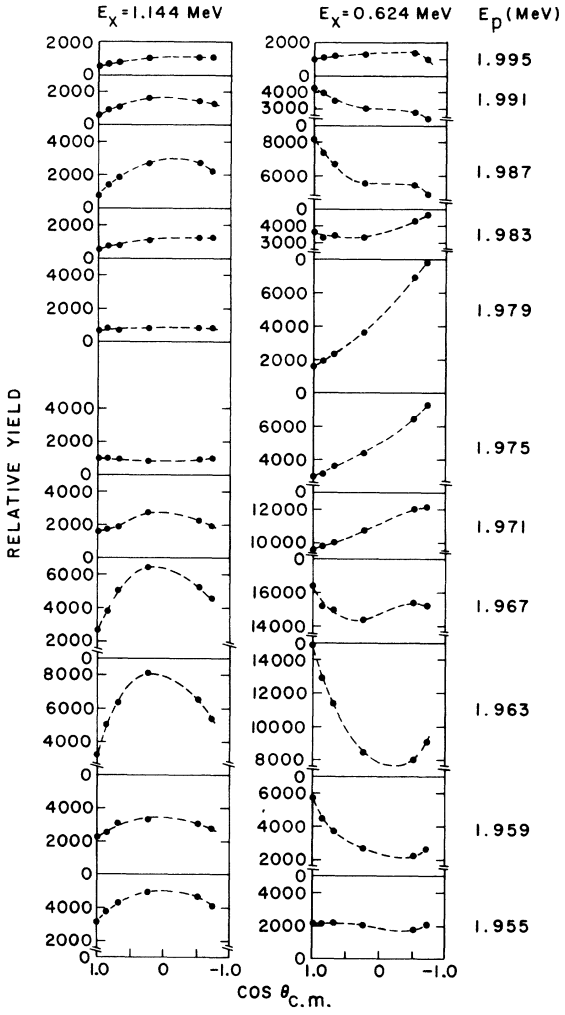


FIG. 6. Relative differential cross sections in the c.m. system as a function of $\cos\theta_{c.m.}$ for the neutron groups corresponding to the excitation of the $3^+$ (0.624-MeV) state and the $2^+$ (1.144-MeV) state in $^{48}$Sc in the $^{48}$Ca$(p,n)$ reaction at the indicated incident proton energies $E_p$. The smooth curves are drawn only to guide the eye.

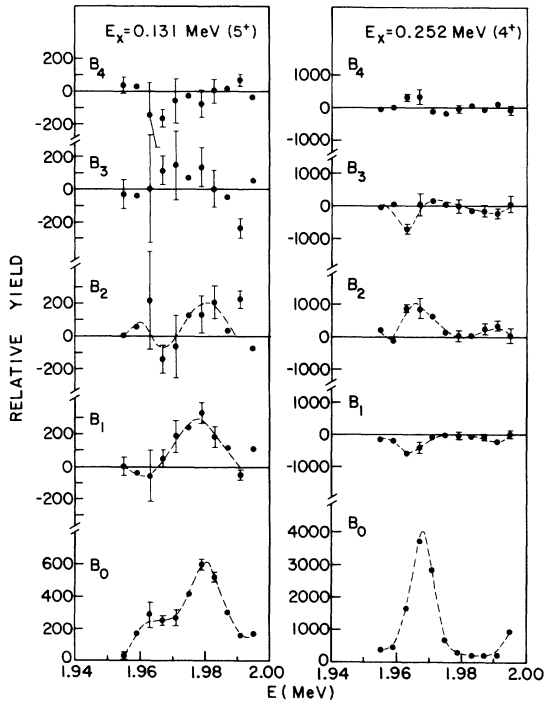


FIG. 7. The coefficients $B_L$ (in the c.m. system) in the expansion of the neutron differential cross sections into a series of Legendre polynomials. They are plotted as a function of laboratory proton energy for the $5^+$ (0.131-MeV) state and the $4^+$ (0.252-MeV) state in $^{48}$Sc. The smooth curves are drawn only to guide the eye.

and proton penetrabilities would predict that the yields near a proton energy of 1.965 MeV would be down by a factor of 15 from those actually observed. On this basis, therefore, as well as from a more complete analysis of the angular distributions, the $(p, n)$ reaction to the $4^+$ state is seen to be dominated by positive-parity resonant states rather than by the $T_<$ $\frac{3}{2}^-$ analog state components. As discussed in Sec. V A, it appears likely that the positive-parity states have $J^\pi = \frac{3}{2}^+$.

As was mentioned in Sec. II, the neutrons associated with the $6^+$ ground state of $^{48}$Sc, the $7^+$ excited state at 1.096 MeV, and the negative-parity state at 1.402 MeV were not observed. For the case of the two positive-parity states, neutron decay from compound-nucleus resonances with $J^\pi \leq \frac{5}{2}^+$ would require partial waves with $l \geq 4$ and would thus be strongly inhibited at the energies involved in the reaction. In the decay to the (probably) $2^-$ final state, the reaction (though the $\frac{3}{2}^-$ resonances) should proceed quite readily by $s$-wave neutron emission; however, the emitted neutrons have an energy of ≈20 keV, which is well below the detector threshold. Consequently, they would not have been observed in these measurements.

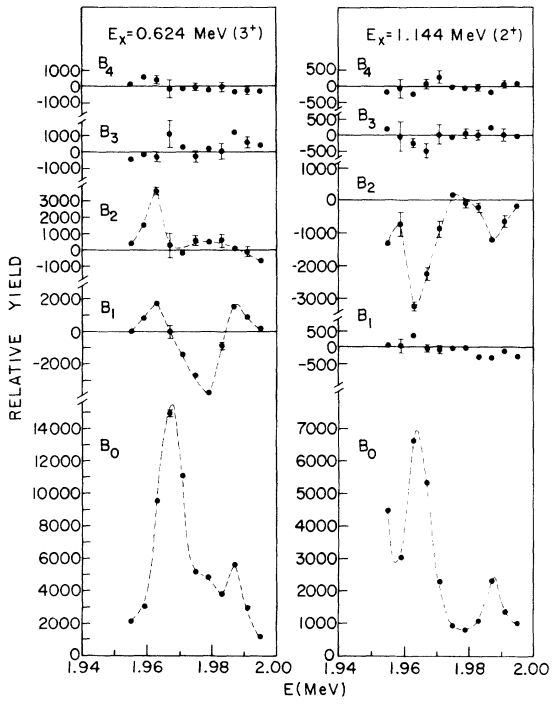


FIG. 8. The coefficients $B_L$ (in the c.m. system) in the expansion o the neutron differential cross sections into a series of Legendre polynomials. They are plotted as a function of laboratory proton energy for the $3^+$ (0.624-MeV) state and the $2^+$ (1.144-MeV) state in $^{48}$Sc. The smooth curves are drawn only to guide the eye.

## IV. THEORY

We consider the present $^{48}$Ca$(p, n)^{48}$Sc data in terms of a single analog state plus a background of two nonoverlapping $\frac{3}{2}^-$ $T_<$ states in the compound system $^{49}$Sc.

The collision matrix elements that describe this process are obtained from the results given by Robson and Lane.[8] In addition to the Hamiltonian $H$ and physical boundary-matching operator $L$ that define the states of the compound system, these authors introduce an "ideal" Hamiltonian $H^0$ and boundary-matching operator $L^0$ such that the eigenstates of $H^0 + L^0$ are the "ideal" analog states $|\lambda\rangle$ and the normal $T_<$ states $|\mu\rangle$.

The Green's function operator for the ideal system is

$$(H^0 + L^0 - E)^{-1} \equiv G^0 = \sum_\lambda \frac{|\lambda\rangle\langle\lambda|}{E_\lambda - E} + \sum_\mu \frac{|\mu\rangle\langle\mu|}{E_\mu - E}, \quad (1)$$

which we write as

$$G^0 = G_1^0 + G_2^0. \quad (2)$$

The corresponding operator

$$(H + L - E)^{-1} \equiv G \quad (3)$$

for the physical system is given in terms of $G_1^0$ and $G_2^0$ by the relation

$$G = G_1 + (1 - G_1 h)(1 + G_2^0 h')^{-1} G_2^0 (1 - h G_1), \quad (4)$$

where

$$G_1 = (1 + G_1^0 h)^{-1} G_1^0, \quad (5)$$

$$h = (H - H^0) + (L - L^0), \quad (6)$$

$$h' = h(1 + G_1^0 h)^{-1}. \quad (7)$$

For our present purpose it is convenient to introduce the level expansions

$$G_1 = \sum_{\lambda\lambda'} |\lambda\rangle A^{(1)}_{\lambda\lambda'} \langle\lambda'|, \quad (8a)$$

$$(1 + G_2^0 h')^{-1} G_2^0 = \sum_{\mu\mu'} |\mu\rangle A^{(2)}_{\mu\mu'} \langle\mu'|, \quad (9a)$$

where $A^{(1)}$ and $A^{(2)}$ are the respective inverses of matrices with elements

$$(E_\lambda - E)\delta_{\lambda\lambda'} + \langle\lambda|h|\lambda'\rangle, \quad (8b)$$

$$(E_\mu - E)\delta_{\mu\mu'} + \langle\mu|h'|\mu'\rangle. \quad (9b)$$

In the notation of Lane and Thomas,[19] the collision matrix $U$ can be written in terms of $G$ as

$$\underline{U} = \underline{\Omega}\,\underline{W}\,\underline{\Omega}, \quad (10)$$

where, if we restrict ourselves to matrix elements $U_{cc'}$ in which both $c$ and $c'$ denote open channels,

$$\underline{W} = \underline{1} + 2i\underline{P}^{1/2}\underline{C}\underline{G}\underline{C}\underline{P}^{1/2}. \quad (11)$$

Here $\underline{\Omega}$ is a diagonal matrix that contains the Coulomb and hard-sphere phase shifts, $\underline{P}$ is the diagonal penetrability matrix, and $\underline{C}$ is a diagonal matrix with elements

$$C_c = (\hbar a_c^2/2M_c)^{1/2}, \tag{12}$$

where $a_c$ is the channel radius and $M_c$ is the reduced mass for channel $c$. For $c \neq c'$, Eq. (11) becomes

$$W_{cc'} = 2i(P_c P_{c'})^{1/2} \langle c | \underline{C} G \underline{C} | c' \rangle, \tag{13}$$

where $|c\rangle$ is the channel wave function $|r_c^{-2}\delta(r_c - a_c)\psi_{as} i^l Y_l\rangle$.

For $(p, n)$ reactions to low-lying ($T_< \frac{1}{2}$) states of the residual nucleus, the isospin of the neutron channel is $T_<$, whereas the isospin of the $|\lambda\rangle$ states is $T_>$. Consequently the states $|\lambda\rangle$ do not contribute to the $n$ channel and Eq. (4) reduces to the form

$$G = (1 + G_2^0 h')^{-1} G_2^0 (1 - hG_1). \tag{14}$$

We could, of course, have assigned the $T_>$ states to $G_2^0$ in Eq. (4), and the $G$ matrix in $n$-$p$ channel space would then have become

$$G = G_1 - G_1 h (1 + G_2^0 h')^{-1} G_2^0 (1 - hG_1). \tag{15}$$

Equations (14) and (15) give equivalent expressions for the $(p, n)$ collision matrix. In Eq. (14) the effects of the analog on the $T_<$ states are explicit, whereas in Eq. (15) the inverse dependence is given explicitly. This has been described more fully by Mello.[7] The representation (14) was chosen for the analysis of the present data.

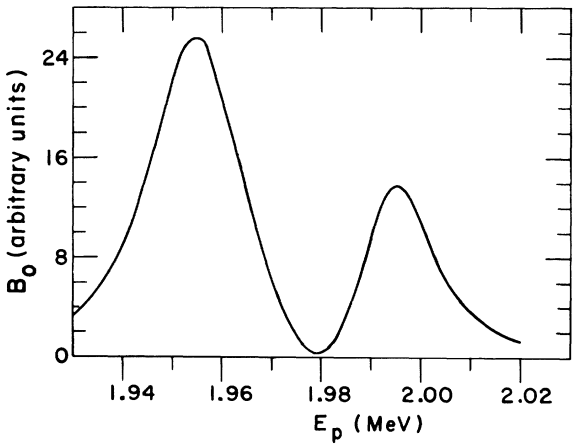


FIG. 9. Calculated neutron yield $B_0$ to a single final state, as obtained with the theory of Sec. IV for a single $T_<$ state in the region of a single analog state. The $T_<$ state is at 1.964 MeV and has a neutron partial width of 3.5 keV and an unenhanced proton width of ~8.5 keV, while the analog state is at 1.986 MeV and its width is ~29.6 keV.

From Eqs. (8a), (9a), and (14) we obtain

$$\langle n | \underline{C} G \underline{C} | p \rangle = \sum_{\mu\mu'} \gamma_{\mu n} A^{(2)}_{\mu\mu'} \alpha_{\mu' p}, \tag{16}$$

where

$$\gamma_{\mu c} = C_c \langle c | \mu \rangle, \tag{17}$$

$$\alpha_{\mu c} = \gamma_{\mu c} - \sum_{\lambda\lambda'} \langle \mu | h | \lambda \rangle A^{(1)}_{\lambda\lambda'} \gamma_{\lambda' c}. \tag{18}$$

The matrix element

$$\langle \mu | h | \lambda \rangle = \langle \mu | H - H^0 | \lambda \rangle + \langle \mu | L - L^0 | \lambda \rangle \tag{19}$$

determines the mixing of $T_>$ and $T_<$ states in the real nucleus, the $H$ and $L$ terms on the right represent interaction mixing and boundary-condition mixing (internal and external mixing), respectively. As shown by Robson,[20]

$$\langle \mu | L - L^0 | \lambda \rangle = -\sum_c L_c \gamma_{\lambda c} \gamma_{\mu c}, \tag{20}$$

where $L_c = S_c + iP_c - b_c$. Here $S_c$ is the usual shift function, $P_c$ the penetrability, and $b_c$ the boundary value for channel $c$. For proton channels $b_p = S_n^-(E - \Delta_C)$, where $S_n^-$ is the (negative-energy) shift function for the charge-exchange channel, and $\Delta_C$ is the Coulomb displacement energy. For $c \neq p$, the value of $b_c$ can be chosen such that $S_c - b_c \approx 0$ for energies in the interval of interest.

Since only a single dominant proton channel contributes to each resonance in the $^{48}$Ca$(p, n)^{48}$Sc reaction, and since $\gamma_{\lambda n} = 0$, Eq. (20) reduces to

$$\sum_c L_c \gamma_{\lambda c} \gamma_{\mu c} = L_p \gamma_{\lambda p} \gamma_{\mu p}. \tag{21}$$

In the case of a single isolated analog resonance, we have from Eqs. (8b), (18), and (21) that

$$\alpha_{\mu p} = \gamma_{\mu p} \frac{E_\lambda - E + \langle \lambda | H - H^0 | \lambda \rangle - \langle \mu | H - H^0 | \lambda \rangle (\gamma_{\lambda p}/\gamma_{\mu p})}{E_A - E - \frac{1}{2} i \Gamma_\lambda}, \tag{22a}$$

where

$$\langle \lambda | h | \lambda \rangle = \Delta_\lambda - \tfrac{1}{2} i \Gamma_\lambda, \tag{22b}$$

$$\Gamma_\lambda = 2 P_p \gamma_{\lambda p}^2, \tag{22c}$$

$$E_A = E_\lambda + \Delta_\lambda. \tag{22d}$$

For the case of two $T_<$ levels in the neighborhood of the analog resonance, Eq. (9b) gives

$$DA^{(2)}_{11} = E_2' - E - \tfrac{1}{2} i \Gamma_2, \quad DA^{(2)}_{22} = E_1' - E - \tfrac{1}{2} i \Gamma_1,$$

$$A^{(2)}_{12} = A^{(2)}_{21} = -h'_{12}/D, \tag{23a}$$

$$D = (E_2' - E - \tfrac{1}{2} i \Gamma_2)(E_1' - E - \tfrac{1}{2} i \Gamma_1) - h_{12}'^2,$$

where for $\mu = 1, 2$

$$\Gamma_\mu = -2 \,\mathrm{Im} \langle \mu | h' | \mu \rangle = 2 \sum_c P_c |\alpha_{\mu c}|^2, \tag{23b}$$

$$E_\mu' = E_\mu + \mathrm{Re} \langle \mu | h' | \mu \rangle, \tag{23c}$$

$$h'_{\mu\nu} = \langle \mu | h' | \nu \rangle = \langle \mu | h | \nu \rangle - \frac{\langle \mu | h | \lambda \rangle \langle \lambda | h | \nu \rangle}{E_A - E - \frac{1}{2} i \Gamma_\lambda}. \tag{23d}$$

If the mixing due to $H - H^0$ is ignored, Eq. (23d) reduces to

$$h'_{\mu\nu} = -i \sum_{c \neq p} P_c \gamma_{\nu c} \gamma_{\mu c} - \frac{L_p \gamma_{\mu p} \gamma_{\nu p} (E_\lambda - E)}{E_A - E - \frac{1}{2} i \Gamma_\lambda} \qquad (24a)$$

and the quantity $\Delta_\lambda$ in Eq. (22b) is given as

$$\Delta_\lambda = -(S_p - S_n^-) \gamma_{\lambda p}^2 . \qquad (24b)$$

## V. DISCUSSION

### A. Comparison with Data

Initial calculations were based on the assumption of a single $\frac{3}{2}^-$ $T_<$ state[21] in the neighborhood of a $\frac{3}{2}^-$ analog state. With all matrix elements of $H - H^0$ set equal to zero, the collision matrix elements for the $(p, n)$ reactions to various final states were calculated by use of Eqs. (13), (16), (22a), and (23a). The energy dependence of the total yield $B_0$ predicted in such a calculation is illustrated in Fig. 9. In this calculation $E'_1$ (lab) = 1.964 MeV and $E_A$ (lab) = 1.986 MeV. An interesting result is the existence of two peaks, one occuring near the energy of the $T_<$ state and the second in the vicinity of $E_A$. The magnitudes and positions of the peaks depend upon the relative energies of the two states as well as on the values of the partial-width amplitudes specified in the calculation. The characteristic asymmetric shape of such calculated curves arises from the energy dependence associated with the enhancement factor given in Eq. (22a).

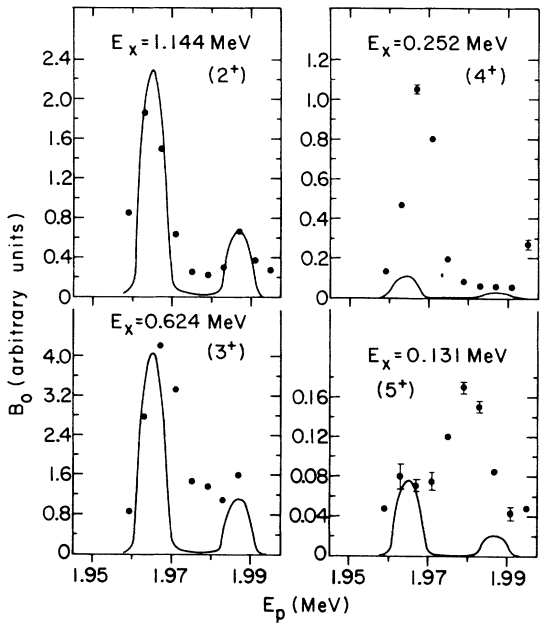


FIG. 10. Comparison between the measured yields $B_0$ (points) and the calculated curve based on the theory of Sec. IV for a single $T_<$ state in the neighborhood of an analog state. The $T_<$ state is at 1.964 MeV, the analog is at 1.986 MeV, and the various partial-width amplitudes are discussed in the text. The experimental resolution was approximated by a Gaussian-shaped curve that was truncated at its half-height and included as a smearing function in the calculations.

These general characteristics of calculations based on the assumption of a single $T_<$ state in the region of an analog resonance are consistent with the gross features of the measured yields (Figs. 7 and 8) for the excitation of the $2^+$ final state (and perhaps the $3^+$). Figure 10 compares the data with these calculations. The $T_<$ state is at an energy $E'_1$ (lab) = 1.964 MeV. Since absolute cross sections were not measured, absolute neutron and proton widths could not be determined. Nevertheless, relative neutron widths in the decay to the various final states have significance in these and in the subsequent calculations discussed below. In the calculations shown in Fig. 10, the neutron reduced-width amplitudes, $\gamma_{1n}$, in the decay to all final states were set equal to each other. The analog state in these calculations was placed at $E_A$ (lab) = 1.986 MeV and was assigned a total proton width $\Gamma_\lambda$ between 0.6 and 1.2 keV. These values are less than the value 1.9 keV given in Ref. 6.

As can be seen, the agreement between the measured yields and those calculated for the excitation of the $2^+$ residual state is fairly good. In fact, the complete measured differential cross section for the reaction to this state can be fitted acceptably on the basis of a model of a single $T_<$ resonance in the neighborhood of an analog. However, at least some of the features of the measured yield to the $3^+$ state and to the $5^+$ state are not reproduced in this calculation. Furthermore, the angular distributions calculated on the basis of a single $T_<$ resonance do not correspond to those measured in the excitation of the $4^+$ state at 0.252 MeV in $^{48}$Sc.

The major features of all of the neutron angular distributions associated with the four final states that were measured can be reproduced quite successfully by means of a more detailed calculation. Figure 11 compares the experimental coefficients $B_0$, $B_1$, and $B_2$ with the results of a calculation that (a) included not only the $T_<$ resonance near $E'_1$ (lab) = 1.964 MeV but also a second $T_<$, $J^\pi = \frac{3}{2}^-$ resonance at $E'_2$ (lab) = 1.986 MeV, (b) moved the $T_>$ (analog) state from $E_A$ (lab) = 1.986 MeV (where it had been in the one-level fit) down to $E_A$ (lab) = 1.978 MeV, and (c) added a few positive-parity states (the necessity for which was discussed in Sec. III). Small changes in $E'_2$ do not substantially affect the agreement with experiment. The width $\Gamma_\lambda$ associated with the analog state was taken to

be somewhat less (i.e., $\Gamma_\lambda = 0.6-1.2$ MeV) than the value given in Ref. 6, although good fits to the data were also found for $\Gamma_\lambda = 1.9$ keV, a value consistent[22] with the results of Ref. 6. A fairly narrow $\frac{5}{2}^+$ resonance, which decays mostly to the $3^+$ and $5^+$ states in $^{48}$Sc, was postulated at a proton energy of 1.978 MeV; and a $\frac{3}{2}^+$ resonance was included at 1.967 MeV. This latter state provides the major contribution to the yield near an energy of 1.965 MeV in the excitation of the $4^+$ final state.

The over-all fit was improved by including a smoothly varying positive-parity contribution to the cross sections throughout the energy region. Within the restrictions of the computer program, this background was represented by a broad $\frac{5}{2}^+$ (total width $\simeq 75$ keV) resonance centered near 2.0 MeV. The unobserved but open channel associated with $s$-wave neutron decay from $\frac{3}{2}^-$ compound-nucleus resonances to the negative-parity (probably $2^-$) final state at 1.402 MeV excitation in $^{48}$Sc was explicitly included in the calculations. A radius $a_c = 1.25A^{1/3}$ fm was used in all calculations.

The computer program was written to handle one or two $T_<$ states, a single $T_>$ state, and one or two non-analog-related states of different $J^\pi$ in which each group of ncn-analog-related states is treated by means of a one- or two-level Breit-Wigner expression. While some of the data could be reproduced by calculations with an assumed analog-state energy different from $E_A$ (lab) = 1.978 ± 0.002 MeV, the best simultaneous fit to all the data could be obtained only for values within this range. This can be compared with the analog-state energy[23] of 1.975 MeV that Wilhjelm *et al.*[6] suggested on the basis of an average of good-resolution measurements, and with the value of 1.980 ± 0.003 MeV used by Jones *et al.*[2] in an analysis of the $^{48}$Ca($p$, $p$) reaction data.

Over all, then, from individual $T_<$ $\frac{3}{2}^-$ components in the energy region near the $\frac{3}{2}^-$ $^{49}$Ca ground-state isobaric analog resonance, the neutron decay to individual final $^{48}$Sc states is consistent with the analysis described in Sec. IV and the assumption of external isospin mixing only. Such a conclusion, although obviously not unique under the present experimental conditions, appears to be the simplest reasonable explanation of the observations: Once the parameters associated with the

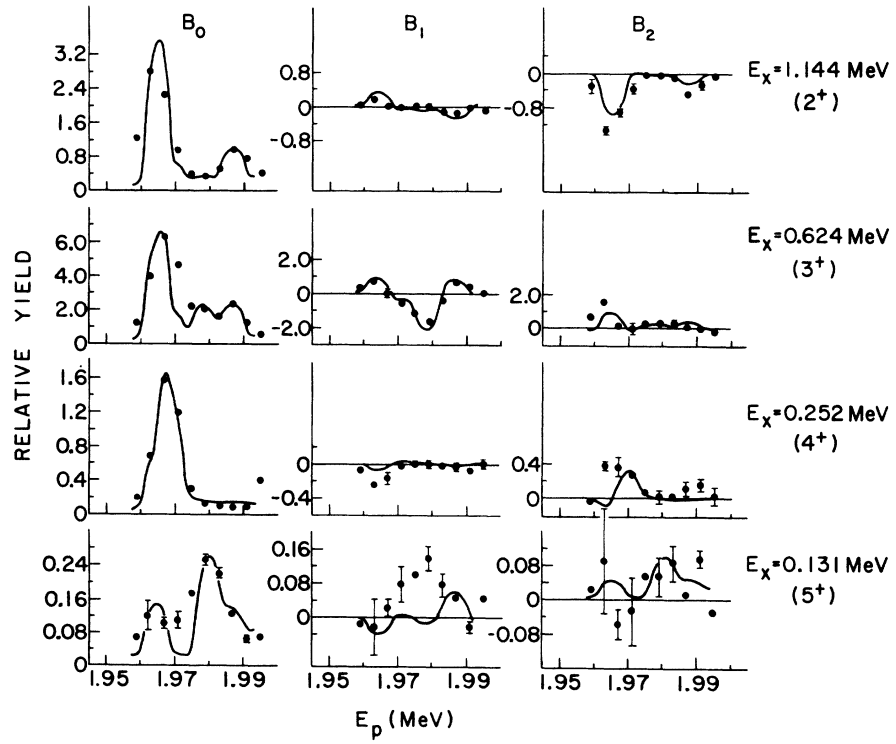


FIG. 11. Comparison between the experimental values of $B_0$, $B_1$, and $B_2$ (points) for transitions to four $^{48}$Sc final states and the curves calculated on the basis of the theory of Sec. IV for two $T_<$ states in the neighborhood of an analog state. Included in this calculation were some positive-parity non-analog-related resonances treated by means of a multilevel Breit-Wigner formula as discussed in the text. The calculations include the effects of the experimental resolution, as mentioned in the caption of Fig. 10.

TABLE I. Branching ratios in the neutron decay from the two main analog components at $E_1'$ (lab) = 1.964 and $E_2'$ (lab) = 1.986 MeV to $^{48}$Sc final states. These results are based on the calculations shown in Fig. 11.

| $E_x$ ($^{48}$Sc) (MeV) | $J^\pi$ | Present results 1.964 | Present results 1.986 | Vingiani *et al.* 1.964 [a] | Vingiani *et al.* 1.986 [b] |
|---|---|---|---|---|---|
| 1.402 | $2^-$ | 0.43 | 0.77 | 0.42 | 0.77 |
| 1.144 | $2^+$ | 0.12 | 0.04 | 0.18 | 0.08 |
| 0.624 | $3^+$ | 0.42 | 0.18 | 0.35 | 0.12 |
| 0.252 | $4^+$ | 0.02 | 0.001 | <0.06 | <0.03 |
| 0.131 | $5^+$ | 0.01 | 0.005 | | |

[a] Represents an average of the branching ratios of Ref. 4 at $E_1'$ (lab) = 1.959 and 1.964 MeV.

[b] Represents an average of the branching ratios of Ref. 4 at $E_2'$ (lab) = 1.975, 1.982, and 1.991 MeV.

analog state are taken as known, this model requires the specification of the fewest number of parameters for other resonances in order to fit the measured differential cross sections.

In the present work we have not really studied the detailed nature of the isospin-mixing process. Because of the rather large beam-energy spread (~8 keV), the observed resonant shapes are governed primarily by the experimental resolution, and consequently any contribution from the internal mixing process in Eqs. (22a) and (23d) may be masked. An attempt to separate the effects of external and internal mixing for the case of a statistical distribution of $T_<$ states has been reported.[24]

### B. Branching Ratios

The branching ratios for neutron decay from the energy region of the two major components associated with the analog state to final states in $^{48}$Sc were obtained from the calculations illustrated in Fig. 11. In Table I these results are compared[25] with the branching ratios of Vingiani *et al.*[4] obtained in an analysis of single-angle yield measurements of both the $^{48}$Ca($p, n\gamma$) and $^{48}$Ca($p, n$) reactions. When the cross sections for the reactions to the final states in $^{48}$Sc are calculated with parameters based on the branching ratios from Ref. 4, the fit to the data is poorer than that shown in Fig. 11.

At $E_1'$ (lab) = 1.964 MeV, about 45% of the neutron decays proceed to the negative-parity state at 1.402 MeV excitation, and the remainder go to the positive-parity final states – mainly the $3^+$ state at 0.624 MeV and the $2^+$ level at 1.144 MeV. On the other hand, at $E_1'$ (lab) = 1.986 MeV, which corresponds to the energy region associated with the largest analog component (as seen, for example, in Fig. 2), approximately 80% of the neutrons decay to the negative-parity state and only 20% to the four positive-parity levels. This increase in the branching ratios to the negative-parity final state at the energy of the largest analog component is *not* due to the fairly rapid increase of the $s$-wave neutron penetrability as the corresponding proton energy is increased from 1.96 to 1.99 MeV. Even when the energy-dependent factors are removed, the branching ratios to the $2^-$ state are about the same as shown in Table I.

These results suggest that the two major $T_< = \frac{7}{2}$ components have somewhat different shell-model configurations. Moreover, these states are probably fairly simple, since, if their configurations were very complicated, approximately equal probabilities for decay to the various low-lying states in $^{48}$Sc would be expected.

The $\frac{3}{2}^-$ analog state in $^{49}$Sc has predominately the 2p-1h configuration $(\pi 1f_{7/2},\ \nu 1f_{7/2}^{-1})^{0^+}\ \nu 2p_{3/2}$, whereas the low-lying positive-parity states in $^{48}$Sc are described by the configuration $(\pi 1f_{7/2},\ \nu 1f_{7/2}^{-1})^{J^\pi}$ with $J^\pi = 0^+, \ldots, 7^+$. The most-likely low-lying negative-parity state of $^{48}$Sc is $(\pi 1f_{7/2},\ \nu 1d_{3/2}^{-1})$.[26,27]

Bloom, McGrory, and Moszkowski[28] have studied the $J^\pi = \frac{3}{2}^-$, $T_< = \frac{7}{2}$ states in $^{49}$Sc that are generated by the configuration $(1f_{7/2})^8(2p_{3/2})$. In particular, these authors conclude that one of these 2p-1h states may have an excitation energy as large as ~10.0 MeV. It is not unreasonable therefore to consider the $T_<$ state at 1.964 MeV ($E_x \approx 11.55$ MeV) in terms of this 2p-1h configuration. However, the present results are not entirely consistent with this interpretation. The calculations reported in Ref. 28 would predict a branching ratio of ~7/1 for $p$-wave neutron decay to the $3^+$ relative to the $2^+$ state in $^{48}$Sc, whereas a ratio of ~3.5/1 is observed. Furthermore, on the basis of this picture alone it would be rather difficult to explain the 0.43 branching ratio for decay to the negative-parity state at 1.402 MeV. On the other hand, this 2p-1h state could be considerably spread amongst core-excited states so that the 2p-1h contribution at 1.964 MeV might be less dominant. The role of 3p-2h configurations might then become relatively more important.

Using a two-body residual interaction consisting of a radial $\Delta$ function with Soper exchange mixture, Divadeenam and Beres[29] find that no 2p-1h states (including those considered by Bloom *et al.*[28]) mix strongly enough with the analog at $E_A$ (lab) = 1.978 MeV to produce observable fragmentation. They further suggest that the fine-structure components of the analog are due to 3p-2h or more complicated couplings. Wilhjelm *et al.*[6] have considered the coupling of 3p-2h states with the same residual interaction and find that very few 3p-2h states couple strongly to the 2p-1h analog. Thus the two

major $T_<$ components could be the result of selective coupling of 3p-2h configurations. This interpretation is made plausible by a level-density calculation[6] which shows that the average level spacing of 3p-2h $\frac{3}{2}^-$ states in the neighborhood of $E_A$ (lab) = 1.978 MeV is ~40 keV. Any specification of the structure of these states, however, presupposes more detailed calculations than have been carried out to date.

---

†Work performed under auspices of U. S. Atomic Energy Commission.

*Present address: University of Chicago, Chicago, Illinois.

‡On leave 1971–72 at Ohio University, Athens, Ohio 45701.

§Also at Ohio University, Athens, Ohio 45701.

[1]See, for example, D. Robson, J. D. Fox, P. Richard, and C. F. Moore, Phys. Letters 18, 86 (1965); H. J. Kim and R. L. Robinson, Phys. Rev. 151, 920 (1966).

[2]K. W. Jones, J. P. Schiffer, L. L. Lee, A. Marinov, and J. L. Lerner, Phys. Rev. 145, 894 (1966).

[3]G. Chilosi, R. A. Ricci, and G. B. Vingiani, Phys. Rev. Letters 20, 159 (1968); G. B. Vingiani, G. Chilosi, and W. Bruynestein, Phys. Letters 26B, 285 (1968).

[4]G. B. Vingiani, R. A. Ricci, R. Giacomich, and G. Poiani, Nuovo Cimento 57B, 453 (1968).

[5]C. Chasman, K. W. Jones, R. A. Ristinen, and J. T. Sample, Phys. Rev. Letters 18, 219 (1967).

[6]P. Wilhjelm, G. A. Keyworth, J. C. Browne, W. P. Beres, M. Divadeenam, H. W. Newson, and E. G. Bilpuch, Phys. Rev. 177, 1553 (1969).

[7]P. A. Mello, Ann. Phys. (N.Y.) 45, 240 (1967).

[8]D. Robson and A. M. Lane, Phys. Rev. 161, 982 (1967).

[9]See, for example, H. Ohnuma, J. R. Erskine, J. P. Schiffer, J. A. Nolen, Jr., and N. Williams, Phys. Rev. C 1, 496 (1970); A. Richter, J. R. Comfort, N. Anantaraman, and J. P. Schiffer, *ibid.* 5, 821 (1972).

[10]A preliminary report of this work was presented by A. J. Elwyn, F. T. Kuchnir, J. E. Monahan, F. P. Mooring, and J. F. Lemming, Bull. Am. Phys. Soc. 16, 556 (1971).

[11]L. M. El-Nadi, O. E. Badawy, A. El-Sourogy, D. A. E. Darwish, and V. Y. Gontchar, Nucl. Phys. 64, 449 (1965); C. Chasman, K. W. Jones, and R. A. Ristinen, Phys. Rev. 140, B212 (1965).

[12]G. Pauletto and F. D. Brooks, Annual Report, Southern Universities Nuclear Institute (SUNI), 1968 (unpublished).

[13]The comparison is with the data of Ref. 6. The energy scale associated with the data of Ref. 6 has been shifted uniformly by 4 keV toward higher energies to match the calibration of the present results.

[14]F. T. Kuchnir and F. J. Lynch, IEEE Trans. Nucl. Sci. NS15, 107 (1968).

[15]Model TC 850 precision time calibrator, Tennelec Company, Oak Ridge, Tennessee.

[16]See, for example, S. M. Austin, Bull. Am. Phys. Soc. 7, 269 (1962); P. R. Bevington, W. W. Rolland, and H. W. Lewis, Phys. Rev. 121, 871 (1961); C. A. Burke, M. T. Lannon, and H. W. Lefevre, Bull. Am. Phys. Soc. 16, 829 (1971); A. Bergström, S. Schwarz, L. G. Strömberg, and L. Wallen, Arkiv Fysik 34, 153 (1967).

[17]B. C. Robertson, I. J. van Heerden, and W. J. McDonald, Nucl. Phys. A176, 193 (1971).

[18]The computer code AUTOFIT is described by J. R. Comfort, Physics Division Informal Report PHY-1970B, Argonne National Laboratory, Argonne, Illinois, August 1970 (unpublished).

[19]A. M. Lane and R. G. Thomas, Rev. Mod. Phys. 30, 257 (1958).

[20]D. Robson, Phys. Rev. 137, B535 (1965); D. Robson, in *Isospin in Nuclear Physics*, edited by J. D. Fox and D. Robson (Academic, New York, 1966), p. 411.

[21]To perform calculations based on a single $\frac{3}{2}^-$ $T_<$ state, set $A^{(2)}_{\mu\mu'} = (E'_1 - E - \frac{1}{2} i\Gamma_1)^{-1}$ in Eq. (16).

[22]For calculations with $\Gamma_\lambda = 1.9$ keV, the relative neutron partial widths in the decay from $\frac{3}{2}^-$ levels to the states in $^{48}$Sc are the same as for the calculations illustrated in Fig. 11.

[23]The energy listed here is 4 keV higher than given in Ref. 6, as explained in Ref. 13.

[24]B. Y. Guzhovskii, D. F. Zaretskii, A. G. Zvenigordoskii, and M. G. Urin, Yadern. Fiz. 13, 719 (1971) [transl.: Soviet J. Nucl. Phys. 13, 409 (1971)].

[25]We assume the comparison is with an *average* of the branching ratios for the fine-structure components observed in Ref. 4.

[26]J. L. Yntema and G. R. Satchler, Phys. Rev. 134, B976 (1964).

[27]S. D. Bloom, private communication.

[28]S. D. Bloom, J. B. McGrory, and S. A. Moszkowski, Nucl. Phys. (to be published).

[29]M. Divadeenam and W. P. Beres, Phys. Rev. Letters 21, 379 (1968).